Characterizing Early-Onset Alzheimer Disease Using Multiprobe PET/MRI

An AT(N) Framework–Based Study

Xiaojun Xu, MS,†‡ Weiwei Ruan, PhD,*†‡ Fang Liu, MD, PhD,*†‡ Qingyao Liu, PhD,*†‡ Yongkang Gai, PhD,*†‡ Ying Su, MD, PhD,§ Zhihou Liang, MD, PhD,§ Xun Sun, MD, PhD,*†‡ and Xiaoli Lan, MD, PhD*†‡*

Purpose: Early-onset Alzheimer disease (EOAD) is rare, highly heterogeneous, and associated with poor prognosis. This AT(N) Framework–based study aimed to compare multiprobe PET/MRI findings between EOAD and late-onset Alzheimer disease (LOAD) patients and explore potential imaging biomarkers for characterizing EOAD.

Methods: Patients with AD who underwent PET/MRI in our PET center were retrospectively reviewed and grouped according to the age at disease onset: EOAD, younger than 60 years; and LOAD, 60 years or older. Clinical characteristics were recorded. All study patients had positive β-amyloid PET imaging; some patients also underwent ^{18}F-FDG and ^{18}F-florzolotau PET. Imaging of the EOAD and LOAD groups was compared using region-of-interest and voxel-based analysis. Correlation of onset age and regional SUV ratios were also evaluated.

Results: One hundred thirty-three patients were analyzed (75 EOAD and 58 LOAD patients). Sex ($P = 0.515$) and education ($P = 0.412$) did not significantly differ between groups. Mini-Mental State Examination score was significantly lower in the EOAD group (14.32 ± 6.74 vs 18.67 ± 7.20, $P = 0.004$). β-Amyloid deposition did not significantly differ between groups. Glucose metabolism in the frontal, parietal, precuneus, temporal, occipital lobe, and supramarginal and angular gyri was significantly lower in the EOAD group (n = 49) than in the LOAD group (n = 44). In voxel-based morphometry analysis, right posterior cingulate/precuneus atrophy was more obvious in the EOAD ($P < 0.001$), although no voxel survived family-wise error correction. Tau deposition in the precuneus, parietal lobe, and angular, supramarginal, and right middle frontal gyri was significantly higher in the EOAD group (n = 18) than in the LOAD group (n = 13).

Conclusions: Multiprobe PET/MRI showed that tau burden and neuronal damage are more severe in EOAD than in LOAD. Multiprobe PET/MRI may be useful to assess the pathologic characteristics of EOAD.

Key Words: ^{18}F-FDG, amyloid PET, early-onset Alzheimer disease, PET/MRI, tau PET

(*Clin Nucl Med* 2023;48: 474–482)

Alzheimer disease (AD) is the most common cause of dementia and is characterized by learning and memory impairment, aphasia, agnosia, dysfunction of visual and spatial skills, change in abstract thinking, and gradual impairment of activities of daily living.[1] Age has an impact on AD heterogeneity and is used to classify patients into early- and late-onset forms of the disease. Early-onset AD (EOAD) accounts for approximately 5% to 10% of all AD cases.[2] Although rare, its burden on families and public health systems is considerable. Early-onset AD is not simply late-onset AD (LOAD) at a younger age: clinical manifestations and pathological features substantially differ between the 2 forms.[3] Atypical clinical manifestations such as visuospatial, language, and executive dysfunction are more common in EOAD.[3–5] Early-onset AD is also highly heterogeneous, progresses more rapidly, and is associated with worse prognosis.[5] Therefore, early evaluation and diagnosis are critical.

The main pathological features of AD include extracellular β-amyloid (Aβ) plaques and intracellular neurofibrillary tangles and have been detected more than 10 years before symptoms appear.[6,7] Autopsy studies have shown that the pathological burden of Aβ plaques and neurofibrillary tangles is greater in EOAD than in LOAD.[3] The National Institute on Aging and the Alzheimer's Association has recently established the AT(N) Framework for defining AD.[8] This framework is based on biomarkers and applies neuroimaging, including PET and MRI, to visualize and track pathophysiological changes.[6,8,9]

Several studies have reported that EOAD exhibits more severe cortical atrophy, greater reduction in cerebral metabolism, and a higher degree of tau deposition than LOAD.[9–15] However, because of heterogeneity, heredity, and other factors, imaging features may overlap.[14,16] The impact of age at onset on Aβ deposition is controversial. Although several studies have reported that Aβ uptake is similar between EOAD and LOAD,[9,17] others have found that Aβ deposition is higher in certain brain regions in patients with EOAD.[11,18]

An imaging biomarker that reliably characterizes EOAD has not yet been identified. Previous neuroimaging studies in EOAD patients have mostly focused on a single modality or molecular probe. An objective mean of characterizing EOAD would provide considerable benefits from both clinical and research perspectives.

Received for publication November 25, 2022; revision accepted March 3, 2023.

From the *Department of Nuclear Medicine, Union Hospital, Tongji Medical College, Huazhong University of Science and Technology; †Hubei Province Key Laboratory of Molecular Imaging; ‡Key Laboratory of Biological Targeted Therapy, the Ministry of Education; and §Departments of Neurology, Union Hospital, Medical College, Huazhong University of Science and Technology, Wuhan, China

Conflicts of interest and sources of funding: This work was supported by the National Natural Science Foundation of China (no. 81701759 and 81901735) and the Key Project of Hubei Province Technical Innovation (2017ACA182). All authors declare that they have no conflict of interest.

Authorship Contributions: X.L. and X.S. conceived and designed the study; W.R. acquired the PET/MRI and provided technique support; Y.G. and Q.L. synthesized probes; Y.S. and Z.L. provided the clinical information and made the diagnosis; X.X. collected and conducted the statistical analysis; F.L. contributed in the reviewed the data; X.X. wrote the manuscript; and X.L. and X.S. reviewed and revised the manuscript. All the authors reviewed and approved the final version of the article.

Supplemental digital content is available for this article. Direct URL citation appears in the printed text and is provided in the HTML and PDF versions of this article on the journal's Web site (www.nuclearmed.com).

Correspondence to: Xiaoli Lan, MD, PhD, Jiefang Ave 1277, Wuhan, Hubei Province 430022, China. E-mail: xiaoli_lan@hust.edu.cn; Xun Sun, MD, PhD, Jiefang Ave 1277, Wuhan, Hubei Province 430022, China. E-mail: xun_sun@hust.edu.cn.

ISSN: 0363-9762/23/4806–0474
DOI: 10.1097/RLU.0000000000004663

This study aimed to compare multiprobe PET/MRI findings between EOAD and LOAD patients and explore potential imaging biomarkers for characterizing EOAD.

PATIENTS AND METHODS

Subjects

The study was approved by the Ethics Committee of Union Hospital Affiliated Tongji Medical College, Huazhong University of Science and Technology (2019-S1208) and registered at ClinicalTrials.gov (NCT05003830). All patients and/or their families provided written informed consent.

Inclusion criteria included AD diagnosis according to the 2011 National Institute on Aging and the Alzheimer's Association diagnostic criteria[19] and positive Aβ PET imaging by visual assessment. Patients with significant cerebrovascular disease (multiple or extensive cerebral infarction), dementia due to other reasons (such as Dementia with Lewy bodies, Parkinson disease with dementia, and so on) or other cognitive dysfunction, history of substance abuse or dependence, and history of epilepsy were excluded. At least 1 integrated PET/MRI was performed for each patient. The authors also excluded patients with claustrophobia, those who could not cooperate with the PET/MRI, and patients whose scans were of poor quality due to movement artifact. The time span for patients' selection was from October 2017 to December 2021. The study flowchart is shown in Figure 1A.

Clinical Evaluation

Data regarding sex, age, age at AD onset, and education level were recorded. Cognitive function was assessed using the Mini-Mental State Examination (MMSE). Patients were grouped according to age at disease onset: EOAD, onset before age 60 years; and LOAD, onset at age 60 years or after. Clinical assessments were performed by 2 experienced neurologists.

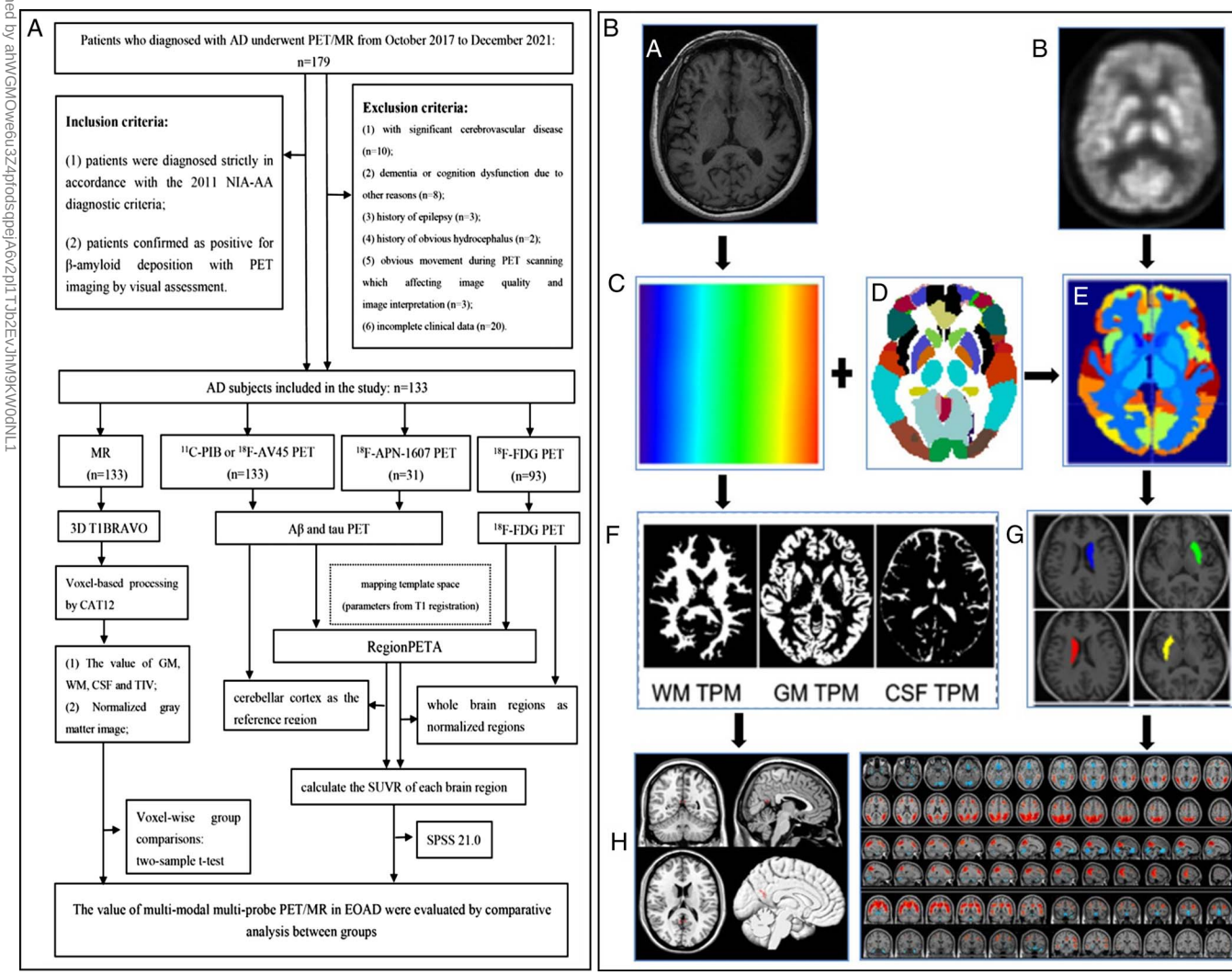

FIGURE 1. Flowchart for screening of AD patients (**A**) and processing of PET/MRI scans (**B**). B, PET and MRI scan analysis processing steps: (**A**, **B**) format conversion of original PET and MRI scans. **C**, T1 image generates the inverse deformation matrix with linear transformation. **D** and **E**, The individualized atlas template construction. **F**, T1 images were segmented to acquire GM, WM, and CSF. **G**, The regions of interest extraction and image analysis. **H**, The results visualization. GM, gray matter; WM, white matter; CSF, cerebrospinal fluid.

PET Imaging Probes

Four imaging probes, ^{11}C-Pittsburgh compound B (PIB), ^{18}F-AV45, ^{18}F-FDG, and ^{18}F-florzolotau (previously known as ^{18}F-APN 1607), were produced in our PET center (radiochemical purity >95%). Detailed methods of preparation are listed in the Supplemental Digital Content, (http://links.lww.com/CNM/A421).

Before imaging, nervous system–related drugs were stopped for more than 12 hours. For ^{18}F-FDG PET, patients fasted for more than 6 hours before the scan; imaging was performed, provided patient blood glucose concentration was less than or equal to 200 mg/L. All probes were administered intravenously (3.7–5.5 MBq/kg). Amyloid PET imaging (^{11}C-PIB or ^{18}F-AV45) was acquired 50 minutes after injection and collected for a total of 20 minutes. ^{18}F-FDG imaging was acquired approximately 45 minutes after for 15 minutes, and tau imaging was acquired 90 minutes after for 20 minutes.

Image Acquisition and Reconstruction

PET was performed using a 3.0 T hybrid time-of-flight PET/MRI scanner (SIGNA; GE Healthcare, Chicago, IL) or PET/CT scanner (Discovery VCT; GE Healthcare). All scans were completed within 2 months for each patient. PET was performed in 3-dimensional (3D) acquisition mode.

For PET/MRI, the total scanning time for PET was 15 minutes. MRI scanning sequence included 3D T1-weighted imaging, T2-weighted imaging, T2-FLAIR, diffusion-weighted imaging, susceptibility-weighted imaging, and 3D-arterial spin labeling. Based on the time-of-flight technique, the PET data were reconstructed using the ordered subset expectation maximum algorithm. The PET attenuation correction was atlas-based MRI attenuation correction, combined with Dixon water-fat separation methods.

For PET/CT, CT scanning was performed after a CT scout view (tube voltage, 120 kV; tube current, 110 mAs; scan thickness, 3.75 mm). PET image was reconstructed using a 3D ordered subset expectation maximum algorithm. A low-dose CT transmission scan was performed for attenuation correction.

Image Preprocessing and Analysis

The preprocessing workflow for PET/MRI images is shown in Figure 1B. Original images were in Digital Imaging and Communications in Medicine format. Preprocessing was performed using the Statistical Parametric Mapping 12 package (http://www.fil.ion.ucl.ac.uk/spm) in Matlab2020b (MathWorks, Natick, MA). Specific steps are shown in detail in the Supplemental Digital Content, (http://links.lww.com/CNM/A421). Image analysis was performed using voxel-based group comparison and region of interest (ROI)–based group quantitative analysis.

Voxel-Wise Group Comparison Analysis

The 2-sample *t* test was used to compare variations in cortical atrophy, hypometabolism, and Aβ and tau deposition between the EOAD and LOAD groups with MMSE score as a covariate. Total intracranial volume was used as a covariate in the examination of cortical atrophy. The resulting t-maps were displayed on a Montreal Neurological Institute template brain with significance threshold set at $P < 0.001$. Family-wise error (FWE) correction at the cluster level was applied for multiple comparisons with a significance threshold of $P < 0.05$. If the cluster size was less than 30 voxels, it was eliminated as noise. The Montreal Neurological Institute coordinates of the local maximum of each cluster were converted into Talairach coordinates.

ROI-Based Group Quantitative Analysis

The mean SUV (SUV_{mean}) and SUV ratio (SUVR) of each region were obtained as previously described.[20,21] β-Amyloid or tau PET and ^{18}F-FDG PET images were normalized using cerebellar cortex and whole-brain mean values, respectively. β-Amyloid PET imaging was carried out with ^{11}C-PIB or ^{18}F-AV45.

Statistical Analysis

Continuous variables are expressed as means with SD. Categorical variables are expressed as percentages. The independent-sample *t* test or Mann-Whitney *U* test was used to compare regional SUVR and clinical parameters between groups as appropriate. Comparison between sexes was performed using the χ^2 test. Pearson or Spearman analysis was used to assess the correlation between SUVR of ROIs and onset age. $P < 0.05$ was considered significant. Statistical analyses were performed using SPSS software version 21.0 (IBM Corp, Armonk, NY).

RESULTS

Patient Characteristics

One hundred thirty-three AD patients were included for analysis. Patient characteristics are shown in Table 1. The EOAD group comprised 75 patients, and the LOAD group comprised 58. Although sex ($\chi^2 = 0.424$, $P = 0.515$) and education level ($P = 0.412$) did not significantly differ between the groups, MMSE score was significantly lower in the EOAD group ($P = 0.004$).

Structural Changes on MRI

The EOAD group had no more severe atrophy region compared with the LOAD group after FWE correction ($P > 0.05$). In contrast, the LOAD group showed a higher left anterior cerebellar lobe atrophy than the EOAD group ($P = 0.004$). Detailed results

TABLE 1. Demographic and Clinical Parameters of Alzheimer Disease Patients

Characteristics	Mean ± SD	Range	Grouping		*P*
			EOAD (n = 75)	LOAD (n = 58)	
Sex					
Male	50		30 (22.6%)	20 (15.0%)	0.515
Female	83		45 (33.8%)	38 (28.6%)	
Age at onset, y	58.93 ± 8.53	35–79	52.72 ± 4.56	66.98 ± 4.96	0.000
Age at PET scan, y	62.08 ± 8.03	42–81	56.49 ± 4.84	69.29 ± 4.97	0.000
Education, y	9.71 ± 4.12	0–22	9.40 ± 4.59	10.10 ± 3.42	0.412
MMSE score	16.22 ± 7.25	1–29	14.32 ± 6.74	18.67 ± 7.20	0.004

are shown in Table S1 and Figure S1 (Supplemental Digital Content, http://links.lww.com/CNM/A421).

Aβ Deposition Differences

Amyloid PET imaging was performed using ^{11}C-PIB in 74 patients and ^{18}F-AV45 in 59 patients. ^{11}C-PIB deposition did not significantly differ between the EOAD and LOAD groups. For ^{18}F-AV45 PET uptake, there was also no significant difference after FWE correction at the cluster level. Detailed results are shown in Figure 2.

Differences in Glucose Metabolism

Average SUV_{mean} of the entire cerebral cortex did not significantly differ between the groups for ^{18}F-FDG ($P = 0.185$). In the quantitative analysis of SUVR in ROIs, glucose metabolism in the frontal lobe, parietal lobe, supramarginal gyrus, angular gyrus, precuneus, temporal lobe, and occipital lobe was lower in the EOAD group (n = 49) than in the LOAD group (n = 44; $P < 0.05$). Hypometabolism in the LOAD patients was predominantly located in the calcarine cortex, medial temporal lobe, lingual gyrus, orbitofrontal cortex, medial temporal lobe (insula, hippocampus, amygdala), anterior cingulate gyrus (ACG), and both basal

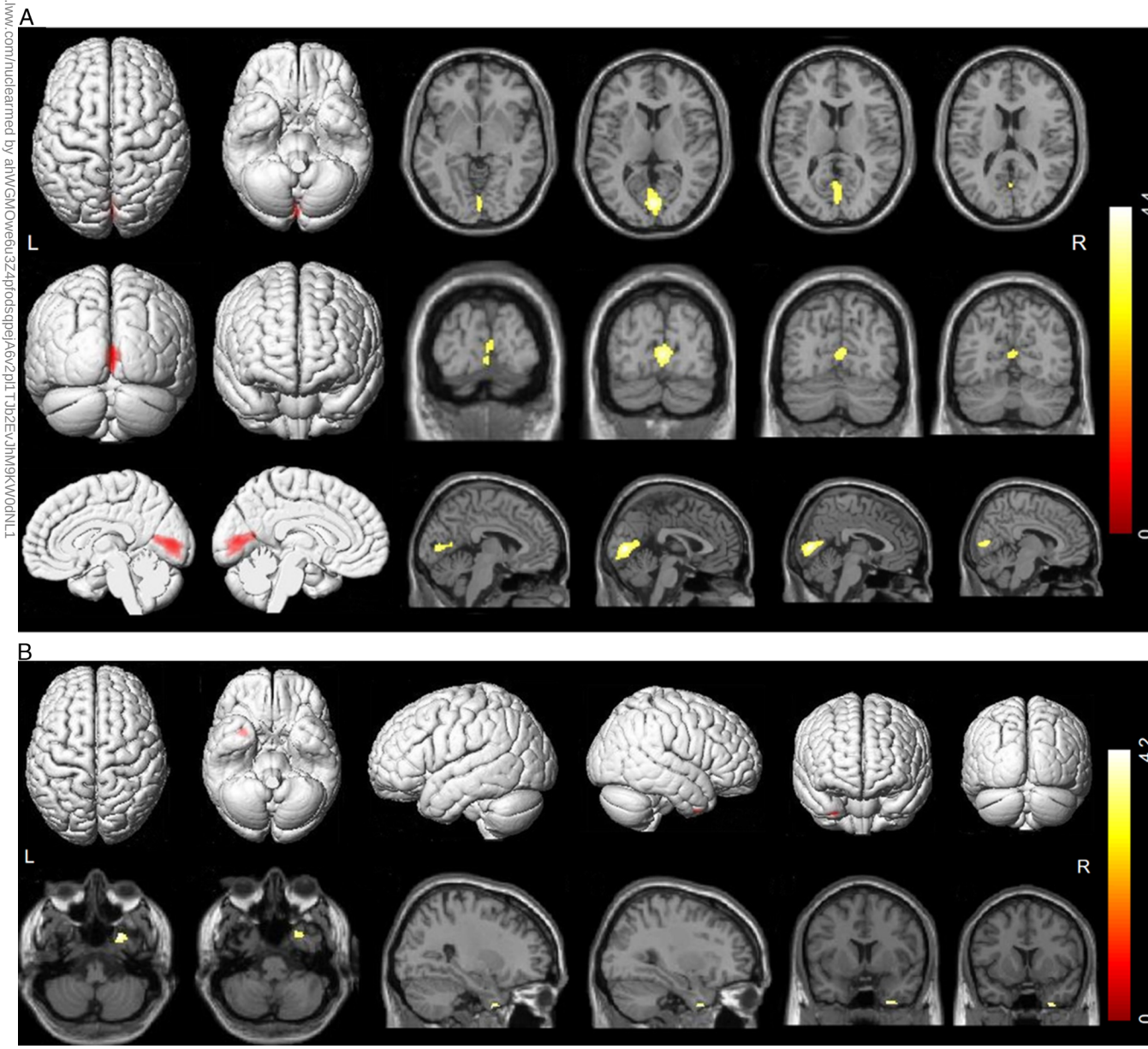

FIGURE 2. Between-group differences of Aβ deposition in EOAD and LOAD. **A**, ^{18}F-AV45 PET result. EOAD patients exhibited higher Aβ deposition in calcarine cortex than LOAD, but did not survive after FWE correction ($P > 0.05$). **B**, ^{11}C-PIB PET result. EOAD patients had a higher ^{11}C-PIB retention in the right superior temporal gyrus, but did not survive after FWE correction ($P > 0.05$). The color bar indicates the *t* value of the cluster.

ganglia and thalami ($P < 0.05$). Detailed results are shown in Table 2 and Figure S2 (Supplemental Digital Content, http://links.lww.com/CNM/A421).

Similar results were obtained in the voxel-group analysis. Glucose metabolism in the superior middle frontal gyrus, parietal lobe, precuneus, superior middle temporal gyrus, and occipital lobe was significantly lower in the EOAD group ($P < 0.05$). The LOAD group showed significant hypometabolism in the cerebellar cortex, orbitofrontal cortex and ACG ($P < 0.05$). Detailed results are shown in Table S2 and Figure 3.

Regional ^{18}F-APN 1607 Uptake Differences

The main brain regions with significant differences in ^{18}F-APN 1607 SUVR between the EOAD (n = 18) and LOAD (n = 13) groups were the right inferior frontal gyrus, right middle cingulate gyrus, right supramarginal gyrus, and right precuneus ($P < 0.05$). Tau deposition was more obvious in the EOAD group. Detailed results are shown in Table 3 and Figure S3 (Supplemental Digital Content, http://links.lww.com/CNM/A421).

In the voxel-wise analysis, tau deposition was significantly higher in the precuneus, parietal lobe, and angular, supramarginal, and right middle frontal gyri of the EOAD group ($P < 0.05$). Detailed results are shown in Table S3 (Supplemental Digital Content, http://links.lww.com/CNM/A421) and Figure 4.

Figure 5 shows the multiprobe PET/MRI or PET/CT fusion images of an EOAD patient and a LOAD patient with comparable clinical severity.

TABLE 2. Comparison of ^{18}F-FDG SUVR of Different ROIs Between EOAD and LOAD

	Grouping		
^{18}F-FDG Region	**EOAD (n = 49)**	**LOAD (n = 44)**	***P***
Frontal lobe			
Rolandic_Oper_R	1.12 ± 0.10	1.08 ± 0.15	0.026
Olfactory_L	0.87 ± 0.14	0.79 ± 0.12	0.000
Olfactory_R	0.89 ± 0.13	0.78 ± 0.13	0.000
Rectus_L	1.02 ± 0.17	0.93 ± 0.14	0.000
Rectus_R	1.07 ± 0.18	0.97 ± 0.17	0.000
Limbic lobe			
ACG_L	0.99 ± 0.12	0.90 ± 0.11	0.001
ACG_R	1.02 ± 0.14	0.94 ± 0.12	0.005
Hippo_L	0.77 ± 0.11	0.71 ± 0.10	0.001
Hippo_R	0.84 ± 0.09	0.77 ± 0.16	0.001
Insula_L	1.01 ± 0.11	0.93 ± 0.13	0.002
Insula_R	1.03 ± 0.10	0.96 ± 0.11	0.002
Amygdala_L	0.78 ± 0.19	0.71 ± 0.12	0.038
Amygdala_R	0.80 ± 0.18	0.73 ± 0.17	0.002
Parietal lobe			
Supramarginal_L	0.93 ± 0.20	1.00 ± 0.22	0.005
Supramarginal_R	0.98 ± 0.16	1.07 ± 0.14	0.000
Angular_L	0.80 ± 0.19	0.99 ± 0.28	0.000
Angular_R	0.86 ± 0.19	1.03 ± 0.18	0.000
Precuneus_L	1.04 ± 0.15	1.15 ± 0.17	0.000
Precuneus_R	1.03 ± 0.14	1.15 ± 0.19	0.000
Parietal_L	0.88 ± 0.17	1.01 ± 0.20	0.000
Parietal_R	0.87 ± 0.17	1.01 ± 0.18	0.000
Temporal lobe			
Fusiform_R	1.05 ± 0.10	0.98 ± 0.15	0.007
Occipital lobe			
Lingual_R	1.24 ± 0.13	1.16 ± 0.15	0.008
Calcarine_L	1.43 ± 0.16	1.33 ± 0.19	0.012
Calcarine_R	1.53 ± 0.17	1.43 ± 0.20	0.017
Occipital_L	1.02 ± 0.18	1.10 ± 0.19	0.036
Occipital_R	1.08 ± 0.16	1.15 ± 0.20	0.048
Basal ganglia			
Caudate nucleus_L	0.92 ± 0.18	0.84 ± 0.21	0.032
Caudate nucleus_R	0.93 ± 0.17	0.81 ± 0.18	0.002
Putamen_L	1.36 ± 0.13	1.25 ± 0.22	0.008

All the data are presented as mean ± SD.
Hippo, hippocampus; L, left; R, right.

Correlation Between Onset Age and SUVR

For Aβ PET, only a few regions showed a weak negative correlation between onset age and SUVR, including left rectus ($r = -0.190$, $P = 0.028$), right olfactory cortex ($r = -0.188$, $P = 0.030$), right insula ($r = -0.216$, $P = 0.013$), the left calcarine cortex ($r = -0.246$, $P = 0.004$), the right calcarine cortex ($r = -0.266$, $P = 0.002$), and right lingual gyrus ($r = -0.233$, $P = 0.007$; Fig. S4 [Supplemental Digital Content, http://links.lww.com/CNM/A421]).

For ^{18}F-FDG, there was obvious correlation in multiple brain regions between onset age and SUVR. A strong positive correlation was found in the parietal lobe, occipital lobe, and posterior cingulate gyrus ($r = 0.205$–0.542, $P < 0.05$). In contrast, a moderate negative correlation was found in the following areas: frontal lobe, ACG, temporal lobe, calcarine, lingual gyrus, basal ganglia, and thalamus ($r = 0.209$ to -0.536, $P < 0.05$). Detailed results are shown in Table S4 and Figure S5 (Supplemental Digital Content, http://links.lww.com/CNM/A421).

Onset age significantly negatively correlated with tau load (SUVR) in multiple regions, mainly including the right inferior frontal gyrus ($r = -0.557$, $P = 0.001$), right cuneus ($r = -0.539$, $P = 0.002$), right supramarginal gyrus ($r = -0.522$, $P = 0.003$), right precuneus ($r = -0.503$, $P = 0.004$), right middle cingulate gyrus ($r = -0.495$, $P = 0.005$), right frontal middle gyrus ($r = -0.473$, $P = 0.007$), and right angular gyrus ($r = -0.459$, $P = 0.009$). Detailed results are shown in Table S5 and Figure S6 (Supplemental Digital Content, http://links.lww.com/CNM/A421).

DISCUSSION

To better characterize EOAD, this study analyzed and compared the multiprobe PET/MRI of patients with EOAD and LOAD. Our results confirmed that multiprobe PET/MRI is effective for diagnosing and assessing AD. Tau and ^{18}F-FDG imaging significantly differed between the EOAD and LOAD groups, but Aβ imaging did not. Based on the AT(N) Framework, these results demonstrate that pathological tau burden and neuronal damage are more severe in EOAD than in LOAD. Tau PET and ^{18}F-FDG PET seem to be better than MRI for characterizing EOAD. Tau deposition and hypometabolism in the parietal lobe and surrounding brain regions (precuneus, angular gyrus, and supramarginal gyrus) were the best imaging features for identifying EOAD. Our findings suggest that the imaging differences between EOAD and LOAD may reflect variations in the distribution of underlying neuropathology. Furthermore, this should assist with early identification of EOAD, which would guide intervention and prognostication.

The distribution and degree of ^{18}F-FDG hypometabolism between EOAD and LOAD significantly differed. Early-onset AD patients had more severe hypometabolism in neocortical regions, which is consistent with previous studies.[14,15,22–26] In patients with comparable dementia severity, hypometabolism was more pronounced in EOAD, which probably reflects greater functional reserve in

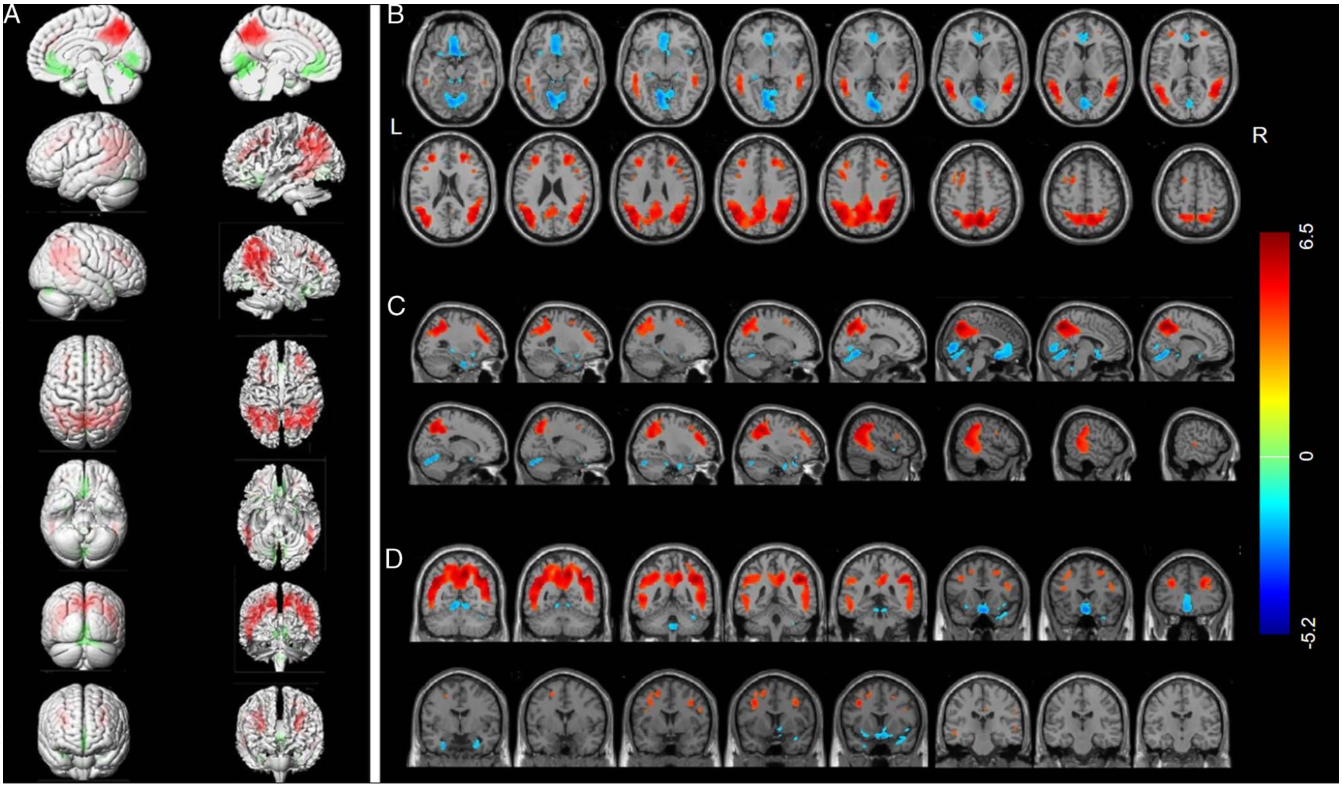

FIGURE 3. Cortical region display of ^{18}F-FDG metabolism difference between EOAD and LOAD groups. **A**, Glass brain images (Render view). **B–D**, Section view images. The difference in specific brain regions shown in axial, sagittal, and coronal planes. The results showed that, compared with LOAD, the EOAD exhibited more severe hypometabolism in the middle frontal gyrus, parietal, occipital, precuneus, superior and middle temporal gyrus (red areas), and hypometabolic regions in LOAD mainly included orbitofrontal cortex, lingual gyrus, calcarine, ACG (blue areas). The color bar indicates the *t* value of the cluster.

younger patients.[23] Hypometabolism was more pronounced in the parietal, lateral temporal, and occipital lobes in EOAD patients, which might be reflected in their clinical symptoms. Early-onset AD patients are more prone to experience nonmemory manifestations, such as impairment of visuospatial function, language, executive function, and attention. Our result is further supported by findings in a previous brain metabolic network study that showed severe extensive reduction of the resting-state network in EOAD patients.[25]

In our study, degree of hypometabolism in the medial temporal lobe was greater in LOAD patients than in EOAD patients, which has been previously reported.[22–24] In addition, metabolism in the ACG and orbitofrontal, lingual, calcarine, and cerebellar cortices was lower in LOAD patients. These findings might be explained by the fact that the primary sensory cortex, motor cortex, visual cortex, ACG, and orbitofrontal cortex are less structurally involved in patients with EOAD.[27,28] Neurodegeneration and neurological damage in the corresponding brain regions might be more severe in LOAD than in EOAD and therefore have greater metabolic defects.

Tau PET effectively detects tau pathology in AD.[6,15,29,30] In our study, a novel tau PET tracer, ^{18}F-APN 1607, was used to evaluate tau deposition. Early-onset AD patients had more pronounced tau deposition in neocortical regions. Age is an important determinant of the degree of cortical tau uptake in AD.[9,31,32] Previous pathological and PET studies have demonstrated that younger subjects exhibit more extensive and severe cortical tau uptake and greater tau pathology.[9,31,33,34] This may reflect that the course of AD at a younger age is more aggressive, so the accumulation rate of tau is faster. Moreover, other pathological mechanisms that can cause cognitive impairment are less common in younger subjects. Therefore, it is possible to maintain a higher pathological burden at the same level of cognitive impairment.[9,31] Tau is closely related to severity of dementia and neuronal damage.[15,29,34] We found that brain regions with more significant tau deposition in EOAD patients,

TABLE 3. A Comparison of Tau PET Uptake Value in EOAD and LOAD

	Grouping		
^{18}F-APN-1607 Region	EOAD (n = 18)	LOAD (n = 13)	*P*
IFG_R	1.33 ± 0.32	1.06 ± 0.26	0.019
MCG_R	1.62 ± 0.53	1.25 ± 0.32	0.032
Supramarginal_R	1.73 ± 0.53	1.35 ± 0.38	0.045
Precuneus_R	1.88 ± 0.60	1.46 ± 0.46	0.041
Palladium_L	1.09 ± 0.18	1.25 ± 0.16	0.015
Palladium_R	1.07 ± 0.21	1.24 ± 0.28	0.025
Thalamus_L	1.17 ± 0.19	1.31 ± 0.16	0.035
Thalamus_R	1.13 ± 0.23	1.28 ± 0.15	0.041

The SUVR are presented as mean ± SD.

IFG, inferior frontal gyrus; L, left; MCG, middle cingulate gyrus; R, right.

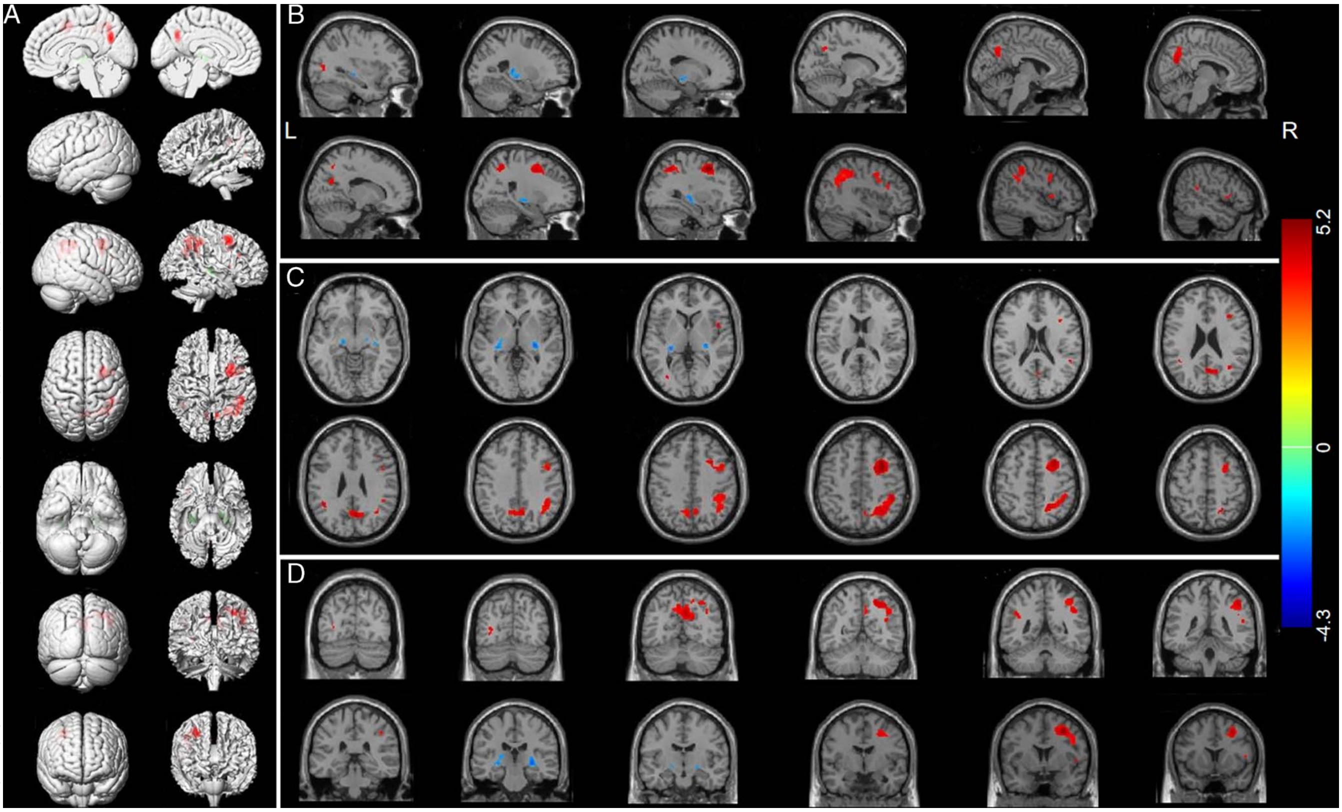

FIGURE 4. Regional ^{18}F-APN-1607 uptake difference in EOAD and LOAD. **A**, Glass brain images (Render view). **B–D**, Section view images. The difference in specific brain regions shown in sagittal, axial, and coronal planes. Right middle frontal gyrus, inferior frontal gyrus, parietal, precuneus, and right supramarginal and right angular gyri showed higher ^{18}F-APN-1607 uptake in patients with EOAD (red areas). LOAD deposited more significantly in the basal ganglia and thalamus (blue areas), but no significant difference after FWE correction (*P* > 0.05). The color bar indicates the *t* value of the cluster.

including the frontal lobe, parietal lobe, precuneus, supramarginal gyrus, and angular gyrus, also exhibited ^{18}F-FDG hypometabolism, suggesting that neuronal hypometabolism in these areas might be affected by tau aggregates.[9]

Our findings have added to the evidence that the parietal lobe is a key region for characterizing EOAD patients.[11,23] We also found that the frontal lobe plays a key role as well and that the performance of different subregions varies greatly. In the middle frontal and inferior frontal gyri, tau deposition and hypometabolism were more significant in EOAD, whereas in the orbitofrontal cortex, they were more significant in LOAD. This might be related to the fact that the prefrontal cortex, with its complex patterns of fiber connections, is a central region that is part of the default mode network, a network that is responsible for higher-order cognitive functions.[35] The value of this region in EOAD needs to be verified and explored further.

Amyloid PET is also an effective biomarker in assessing AD.[7] The diagnostic sensitivity of Aβ PET is comparable to that of autopsy, which is the criterion standard. However, Aβ plaques plateau early in the disease.[31] Conclusive evidence regarding the effect of onset age on Aβ deposition is still lacking. In our study, as in several previous ones,[17,18] β-amyloid deposition did not significantly differ between EOAD and LOAD, indicating no close association between Aβ deposition and onset age. Conversely, others have reported that Aβ deposition is more pronounced in EOAD.[11,18,36,37] The discrepancy might be related to differences in group categorization, sample size, and methodology between studies.

Voxel-based MRI analysis showed no significant difference in cortical atrophy between EOAD and LOAD in our study. However, most previous ones have reported that cortical atrophy is more extensive in EOAD, although the patterns of atrophy varied.[10,22,38,39] Early-onset AD typically showed more parietal involvement, whereas LOAD was associated with more hippocampus atrophy. The inconsistency might be partly due to heterogeneity in study design and data.

This study had several limitations. First, the sample size was small, which limits the ability to draw generalized conclusions. Second, although patients with a family history of AD were excluded, genetic testing was not performed. Some subjects may have had familial AD or familial AD gene mutations. Third, abnormal hypometabolism in calcarine cortex was more often seen in LOAD subjects in this study. This phenomenon is also one of the supportive biomarkers for the diagnosis of dementia with lewy bodies (DLB).[40] Because of the lack of pathological diagnosis of DLB (the presence of "Lewy bodies"), concomitant DLB cannot be totally ruled out in some AD patients. Furthermore, a recently recognized disease, limbic-predominant age-related TDP-43 encephalopathy (LATE), has the same symptoms and neurodegeneration as AD. According to the consensus working group report of LATE,[41] in an A+T-(N)$^{+}$ subject, the N^{+} is likely due to a comorbid non-AD pathology. Although often with hippocampal sclerosis, LATE may have the neurodegeneration shown as atrophy or hypometabolism in medial temporal, which suggests LATE may mimic non-AD comorbidity. Unfortunately, not all Aβ-positive

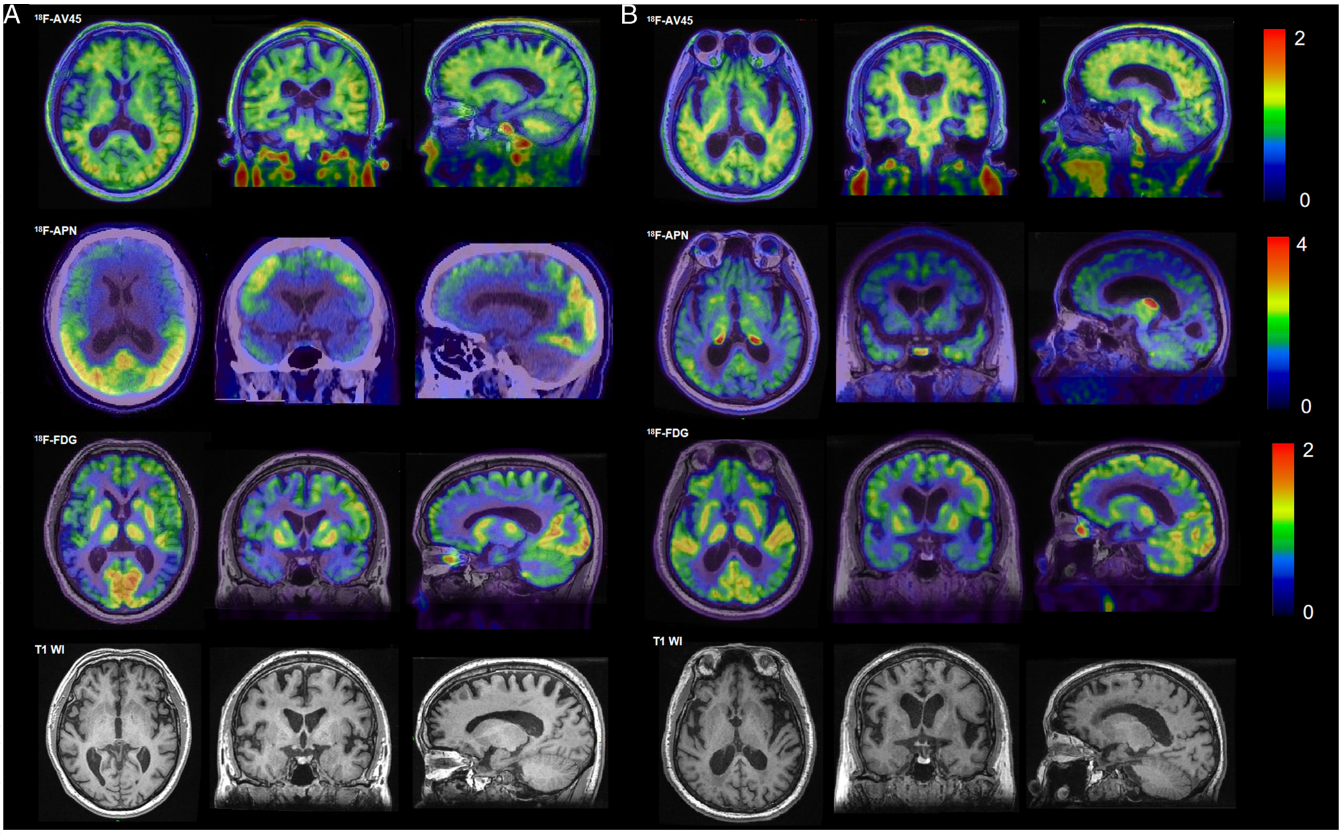

FIGURE 5. Multiprobe PET/MRI/CT fusion images of an EOAD patient and a LOAD patient with comparable clinical severity. **A**, A 51-year-old man complained of memory decline for 2 years (MMSE = 11, 9 years of education). **B**, A 71-year-old man was with amnestic cognitive impairment for 2 years (MMSE = 14, 12 years of education). From top to bottom, the Aβ, tau, ^{18}F-FDG PET, and T1-weighted MRI structural images were shown, respectively. The imaging results of 2 patients were significantly different. β-Amyloid PET illustrated diffusely increased amyloid uptake in the cerebral cortex of 2 patients, but the difference was not significant. ^{18}F-APN-1607 PET demonstrated that tau deposition in EOAD patients was significantly higher, especially in parietal lobe and occipital lobe. Except for occipital lobe, glucose metabolism is reduced in both patients in most neocortex regions, and EOAD was more pronounced. However, MRI revealed slight atrophy in bilateral parietal and medial temporal lobes in EOAD, and LOAD had severe brain atrophy in most of the cerebral cortex. The colored bar indicates SUVR.

patients had tau imaging performed in this study, which limited the differential diagnosis. Finally, this study was performed as a retrospective analysis. Future studies should be conducted longitudinally and explore the association between patterns of impairment in different cognitive domains and imaging features. Brain metabolic network research and application of artificial intelligence technology have great potential to assist in these endeavors.

CONCLUSIONS

Although Aβ PET is useful for accurate diagnosis of AD, it alone is insufficient to differentiate EOAD and LOAD. Based on the AT(N) Framework, pathological tau burden and neuronal damage are more severe in EOAD. Tau PET and ^{18}F-FDG PET seem to be better at characterizing EOAD than Aβ PET. The parietal lobe and surrounding regions are the most prone to tau deposition and hypometabolism in EOAD.

ACKNOWLEDGMENTS

The authors thank the patients and family members who participated in this study. They are grateful for the support from APRINOIA Therapeutics (Suzhou, China), who provided them with precursor and technique instruction for the synthesis of ^{18}F-APN 1607. They also thank J. Ludovic Croxford, PhD, from Liwen Bianji (Edanz) (www.liwenbianji.cn) for editing the language of a draft of this article.

REFERENCES

1. 2020 Alzheimer's disease facts and figures. *Alzheimers Dement*. 2020;16:391–460.
2. Ayodele T, Rogaeva E, Kurup JT, et al. Early-onset Alzheimer's disease: what is missing in research? *Curr Neurol Neurosci Rep*. 2021;21:4.
3. Wattmo C, Wallin AK. Early- versus late-onset Alzheimer's disease in clinical practice: cognitive and global outcomes over 3 years. *Alzheimers Res Ther*. 2017;9:70.
4. Koss E, Edland S, Fillenbaum G, et al. Clinical and neuropsychological differences between patients with earlier and later onset of Alzheimer's disease. *Neurology*. 1996;46:136.
5. Sirkis DW, Bonham LW, Johnson TP, et al. Dissecting the clinical heterogeneity of early-onset Alzheimer's disease. *Mol Psychiatry*. 2022;27:2674–2688.
6. Chandra A, Valkimadi PE, Pagano G, et al. Applications of amyloid, tau, and neuroinflammation PET imaging to Alzheimer's disease and mild cognitive impairment. *Hum Brain Mapp*. 2019;40:5424–5442.
7. Cho H, Choi JY, Hwang MS, et al. In vivo cortical spreading pattern of tau and amyloid in the Alzheimer disease spectrum. *Ann Neurol*. 2016;80:247–258.

8. Jack CR Jr., Bennett DA, Blennow K, et al. NIA-AA research framework: toward a biological definition of Alzheimer's disease. *Alzheimers Dement*. 2018;14:535–562.
9. Koychev I, Gunn RN, Firouzian A, et al. PET tau and amyloid-beta burden in mild Alzheimer's disease: divergent relationship with age, cognition, and cerebrospinal fluid biomarkers. *J Alzheimers Dis*. 2017;60:283–293.
10. Lee EC, Kang JM, Seo S, et al. Association of subcortical structural shapes with tau, amyloid, and cortical atrophy in early-onset and late-onset Alzheimer's disease. *Front Aging Neurosci*. 2020;12:563559.
11. Ossenkoppele R, Zwan MD, Tolboom N, et al. Amyloid burden and metabolic function in early-onset Alzheimer's disease: parietal lobe involvement. *Brain*. 2012;135:2115–2125.
12. Stage EC Jr., Svaldi D, Phillips M, et al. Neurodegenerative changes in early- and late-onset cognitive impairment with and without brain amyloidosis. *Alzheimers Res Ther*. 2020;12:93.
13. Apostolova LG, Aisen P, Eloyan A, et al. The Longitudinal Early-Onset Alzheimer's Disease Study (LEADS): framework and methodology. *Alzheimers Dement*. 2021;17:2043–2055.
14. Aziz AL, Giusiano B, Joubert S, et al. Difference in imaging biomarkers of neurodegeneration between early and late-onset amnestic Alzheimer's disease. *Neurobiol Aging*. 2017;54:22–30.
15. Tanner JA, Iaccarino L, Edwards L, et al. Amyloid, tau and metabolic PET correlates of cognition in early and late-onset Alzheimer's disease. *Brain*. 2022;145:4489–4505.
16. Szigeti K, Doody RS. Should EOAD patients be included in clinical trials? *Alzheimers Res Ther*. 2011;3:4.
17. Rabinovici GD, Furst AJ, Alkalay A, et al. Increased metabolic vulnerability in early-onset Alzheimer's disease is not related to amyloid burden. *Brain*. 2010;133:512–528.
18. Cho H, Seo SW, Kim JH, et al. Amyloid deposition in early onset versus late onset Alzheimer's disease. *J Alzheimers Dis*. 2013;35:813–821.
19. Jack CR Jr., Albert MS, Knopman DS, et al. Introduction to the recommendations from the National Institute on Aging-Alzheimer's Association workgroups on diagnostic guidelines for Alzheimer's disease. *Alzheimers Dement*. 2011;7:257–262.
20. Ruan W, Sun X, Hu X, et al. Regional SUV quantification in hybrid PET/MR, a comparison of two atlas-based automatic brain segmentation methods. *EJNMMI Res*. 2020;10:60.
21. Xu X, Ruan W, Liu F, et al. ^{18}F-APN-1607 tau positron emission tomography imaging for evaluating disease progression in Alzheimer's disease. *Front Aging Neurosci*. 2021;13:789054.
22. Kaiser NC, Melrose RJ, Liu C, et al. Neuropsychological and neuroimaging markers in early versus late-onset Alzheimer's disease. *Am J Alzheimers Dis Other Demen*. 2012;27:520–529.
23. Vanhoutte M, Semah F, Rollin Sillaire A, et al. (18)F-FDG PET hypometabolism patterns reflect clinical heterogeneity in sporadic forms of early-onset Alzheimer's disease. *Neurobiol Aging*. 2017;59:184–196.
24. Kim EJ, Cho SS, Jeong Y, et al. Glucose metabolism in early onset versus late onset Alzheimer's disease: an SPM analysis of 120 patients. *Brain*. 2005;128:1790–1801.
25. Chung J, Yoo K, Kim E, et al. Glucose metabolic brain networks in early-onset vs. late-onset Alzheimer's disease. *Front Aging Neurosci*. 2016;8:159.
26. Tondo G, Iaccarino L, Caminiti SP, et al. The combined effects of microglia activation and brain glucose hypometabolism in early-onset Alzheimer's disease. *Alzheimers Res Ther*. 2020;12:50.
27. Frisoni GB, Pievani M, Testa C, et al. The topography of grey matter involvement in early and late onset Alzheimer's disease. *Brain*. 2007;130:720–730.
28. Pini L, Pievani M, Bocchetta M, et al. Brain atrophy in Alzheimer's disease and aging. *Ageing Res Rev*. 2016;30:25–48.
29. Chételat G, Arbizu J, Barthel H, et al. Amyloid-PET and ^{18}F-FDG-PET in the diagnostic investigation of Alzheimer's disease and other dementias. *Lancet Neurol*. 2020;19:951–962.
30. Pontecorvo MJ, Devous MD Sr., Navitsky M, et al. Relationships between flortaucipir PET tau binding and amyloid burden, clinical diagnosis, age and cognition. *Brain*. 2017;140:748–763.
31. Whitwell JL, Martin P, Graff-Radford J, et al. The role of age on tau PET uptake and gray matter atrophy in atypical Alzheimer's disease. *Alzheimers Dement*. 2019;15:675–685.
32. Smith R, Strandberg O, Mattsson-Carlgren N, et al. The accumulation rate of tau aggregates is higher in females and younger amyloid-positive subjects. *Brain*. 2020;143:3805–3815.
33. Scholl M, Ossenkoppele R, Strandberg O, et al. Distinct ^{18}F-AV-1451 tau PET retention patterns in early- and late-onset Alzheimer's disease. *Brain*. 2017;140:2286–2294.
34. Visser D, Verfaillie SCJ, Wolters EE, et al. Differential associations between neocortical tau pathology and blood flow with cognitive deficits in early-onset vs late-onset Alzheimer's disease. *Eur J Nucl Med Mol Imaging*. 2022;49:1951–1963.
35. Tang H, Bartolo R, Averbeck BB. Reward-related choices determine information timing and flow across macaque lateral prefrontal cortex. *Nat Commun*. 2021;12:894.
36. Choo IH, Lee DY, Kim JW, et al. Relationship of amyloid-β burden with age-at-onset in Alzheimer disease. *Am J Geriatr Psychiatry*. 2011;19:627–634.
37. Li J, Antonecchia E, Camerlenghi M, et al. Correlation of [(18)F]florbetaben textural features and age of onset of Alzheimer's disease: a principal components analysis approach. *EJNMMI Res*. 2021;11:40.
38. Contador J, Perez-Millan A, Tort-Merino A, et al. Longitudinal brain atrophy and CSF biomarkers in early-onset Alzheimer's disease. *Neuroimage Clin*. 2021;32:102804.
39. Contador J, Perez-Millan A, Guillen N, et al. Baseline MRI atrophy predicts 2-year cognitive outcomes in early-onset Alzheimer's disease. *J Neurol*. 2022;269:2573–2583.
40. McKeith IG, Boeve BF, Dickson DW, et al. Diagnosis and management of dementia with Lewy bodies: fourth consensus report of the DLB Consortium. *Neurology*. 2017;89:88–100.
41. Nelson PT, Dickson DW, Trojanowski JQ, et al. Limbic-predominant age-related TDP-43 encephalopathy (LATE): consensus working group report. *Brain*. 2019;142:1503–1527.